metals

MDPI

Article

Recycling Aluminium AA6061 Chips with Reinforced Boron Carbide (B_4C) and Zirconia (ZrO_2) Particles via Hot Extrusion

Sami Al-Alimi [1], Shazarel Shamsudin [1], Nur Kamilah Yusuf [1], Mohd Amri Lajis [1], Wenbin Zhou [2,*], Djamal Hissein Didane [1], Safwan Sadeq [3], Yazid Saif [1], Ahmed Wahib [1] and Zawati Harun [1]

[1] Sustainable Manufacturing and Recycling Technology, Advanced Manufacturing and Materials Center (SMART-AMMC), Universiti Tun Hussein Onn Malaysia, Parit Raja 86400, Malaysia
[2] Department of Mechanical Engineering, Imperial College London, London SW7 2AZ, UK
[3] Department of Mechanical Engineering, Universiti Teknologi Petronas, Seri Iskandar 31750, Malaysia
* Correspondence: w.zhou15@imperial.ac.uk

Abstract: Compared to the recycling process by remelting, hot extrusion significantly reduces the energy consumption and CO_2 emission and ensures good mechanical and microstructural properties. This study investigates the effects of reinforcing aluminium AA6061 chips with mixed boron carbide (B_4C) and zirconia (ZrO_2) particles by employing a design of experiment (DOE) under 550 °C processing temperature and three hours preheating time. The findings showed that compressive strength (CS) and hardness increased with up to 5% added particles, and beyond 5%, the yielded values decreased because of materials agglomeration. However, the decreasing density was dependent on the addition of ZrO_2 particles. The distribution of particles with different volume fractions of mixed particles was investigated by employing SEM, AFM, and EDS tests. Thus, the process can produce a net shape structure that utilises material-bonding consolidation to provide sufficient support to reuse the recovered materials in engineering applications, such as in the automotive industry.

Keywords: solid-state recycling (SSR); hybrid materials; AA6061 chips; boron carbide (B_4C); zirconia (ZrO_2); hot extrusion; design of experiment (DOE)

Citation: Al-Alimi, S.; Shamsudin, S.; Yusuf, N.K.; Lajis, M.A.; Zhou, W.; Didane, D.H.; Sadeq, S.; Saif, Y.; Wahib, A.; Harun, Z. Recycling Aluminium AA6061 Chips with Reinforced Boron Carbide (B_4C) and Zirconia (ZrO_2) Particles via Hot Extrusion. *Metals* **2022**, *12*, 1329. https://doi.org/10.3390/met12081329

Academic Editor: Srecko Stopic

Received: 14 June 2022
Accepted: 25 July 2022
Published: 8 August 2022

1. Introduction

Due to its good combination of characteristics, such as light weight, high strength, and excellent resistance to corrosion, aluminium alloy has been widely utilised in transportation, construction, containers, power supply, and many related applications [1–5]. One efficient way to reduce emissions, such as CO_2, CO, and NOx, during the manufacturing process is to recycle waste materials with less energy consumption. Recycling industrial aluminium wastes also becomes a vital approach for manufacturers to reduce production costs [1]. Traditional recycling methods for aluminium scraps mostly involve remelting and recasting at high-energy usage. However, solid-state recycling (SSR) by forming techniques has been developed to reduce energy consumption during recycling. In this approach, the alloy scraps will undergo plastic deformation below solidus temperature [2]. SSR is a superior concept among light-metal recycling due to its high material recovery and fewer processing steps. The direct conversion process of aluminium machining chips into a finished product by the hot extrusion process was patented by Stern in 1945 to overcome the problem of material loss during the remelting process and reduce energy usage during aluminium production [3]. The SSR by hot extrusion resulted in high strength enhancement of the processed chips due to severe deformation induced during extrusion [6–8]. In addition, SSR by hot extrusion could be cost effective compared to other conventional concepts of material recovery, saving 40% of materials, 31% of energy, and 60% of labour [9,10].

Generally, the performance of the extrudes can be affected by die design, extrusion temperature, and extrusion speed (strain rate) [11–14]. Güley et al. [15] investigated the effect of the die design on the welding quality of the machining chips. The flat-face die and porthole die were employed to produce solid rectangular profiles using AA6060 chips. It was found that the porthole die resulted in better-welded chips, having 80% higher ductility than the flat-face die. Blindheim et al. [16] investigated the continuous extrusion of aluminium alloys via solid-state-bonding extrusion. The process was operated at a temperature lower than the material-melting point to avoid cracking and residual stresses compared to the conventional melting process. Some studies focused on recycling machined chips in hybrid forms reinforced with ceramic particles and compacted in cylindrical bars using the hot extrusion method. Sanusi et al. [17] reported the effects of processing temperature and reinforced particles on the Cu alloy composite structure and properties. Rezaei et al. [18] found that the processing temperature (ranging from room temperature to crystallisation temperature) directly affects the structural properties of Al-Cu-Ti extruded composites. The applied temperature affects the particle distribution and grain size. Higher temperature leads to increased density, hardness, and yield strength. Zhou et al. [19] also reported that increasing the processing temperature improved the distribution of the grains and particles of Mg-Al-1Si alloys. The mechanical properties of the materials were optimum at 330 °C due to the homogenous particle distribution and fine grain size. Nie et al. [20] studied the hot extrusion of 2024 aluminium chips reinforced with boron carbide (B_4C) particulates and found that the elastic modulus and ultimate tensile strength (UTS) of the extrudates were increased by adding B_4C particles into the matrix alloy. The highest UTS value for B_4C/AA2024 composites was 626.7 MPa at 20 vol% B_4C particles, compared to 489 MPa for pure 2024 aluminium alloy. Additionally, a strong interface bonding between B_4C and AA2024 was achieved through mechanical alloying and hot extrusion. Fogagnolo et al. [21] studied the recycling of AA6061 chips reinforced with Al_2O_3 using cold and hot pressing followed by a hot extrusion process. The authors found that the UTS and hardness of the recycled composite material were higher than the primary material producing the chips. Sabbar et al. [10] reviewed the processing of aluminium chips by hot extrusion with and without reinforcing particles. The researcher found that adding reinforced particles has an impact on the material structure and strength properties. Qi et al. [22] investigated the processing of AA6061-T651 commercial alloy by cyclic extrusion process. The electrical conductivity of the processed material increased by 10%, while the hardness slightly dropped. Larianovsky et al. [23] studied the production of Al metal matrix composites reinforced with carbon nanotubes using combined high-pressure die casting (HPDC) and cyclic extrusion (CE). More than 50% efficiency was achieved, and the resulting composites demonstrated improved mechanical properties.

The investigations of aluminium-alloy-based scraps in the pure or composite form are important for reuse of the materials in automotive and aircraft applications [24,25]. AA6061 reinforced with ceramic particles have been widely used in the automotive industry and AA7075 in the aerospace industry. This paper investigated the possibility of recycling aluminium alloy 6061 chips reinforced with B_4C and ZrO_2 particles via hot extrusion. The effects of B_4C and ZrO_2 on the UTS, microhardness, density, and microstructure of the extrudates were studied in detail. The findings will highlight the development of chip-based recycling with multi-reinforced particles towards recycling hybrid material structures.

2. Materials and Methods

2.1. Preparation of the Al6061-B_4C/ZrO_2 Composites

The AA6061-B_4C/ZrO_2 composites were made from AA6061-pulverised chips and B_4C, ZrO_2 ceramic particles. Then, the chips underwent a cleaning process by degreasing with acetone for 30 min in an ultrasonic bath, according to the ASTM G131-96 standard. After cleaning, the chips were dried in an oven at 100 °C for 30 min. Finally, the chips

were mixed with B_4C, ZrO_2 particles using a 3D mixer for 2 h at the speed of 35 rpm. Table 1 summarises the process parameters for preparing the Al6061-B_4C/ZrO_2 composites. The mixing was performed to ensure the distributions between the hybrid materials were uniform. The process depends on the density measurements of both alloys and ceramic constituents. The density of the hybrid materials was determined using the Archimedes' principle, which depends on the densities and volume fractions of the reinforced B_4C, ZrO_2 particles and the AA6061 metal matrix [10,26,27].

Table 1. Process parameters for preparing the Al6061-B_4C/ZrO_2 composites and the subsequent hot extrusion process.

Parameters	Units	Values
Chips size	mm	1
B_4C, ZrO_2 size	μm	7 ± 3
Mixing time	hr	2
Mixing speed	rpm	35
Drying temperature	°C	100
Billet preheated temperature	°C	550
Billet preheated time	hr	3
Extrusion die temperature	°C	300

2.2. Hot-Extrusion Experiment

The direct conversion process of aluminium-machining chips reinforced with B_4C and ZrO_2 particles into a finished product by the hot extrusion process will improve the energy usage of the aluminium production compared with the remelting process. The extrusion process parameters are given in Table 1. The chip-based hybrid reinforced by B_4C and ZrO_2 particles were developed by mixing and blending the chips with the reinforced particles. The composite was cold compacted to produce the billet of 80 mm in length and 30 mm in diameter. After cold compaction, the billet was homogenized in a furnace at 550 °C for 3 h. Subsequently, the hot extrusion of the chip-based composite in the form of a billet was conducted on a hydraulic extrusion press with a maximum extrusion force of 300 tonnes. The billet was preheated to 550 °C to increase the material ductility and deformability. The extrusion die temperature was set at 300 °C. The ram speed was set to 1 mm/s. Each of the extruded profiles were machined by following the ASTM E9 standard to produce the samples for the compressive strength test, carried out with an initial strain rate of 2.53×10^{-3} s^{-1} at room temperature. Figure 1 summarises the experimental methods for material preparation and characterisation.

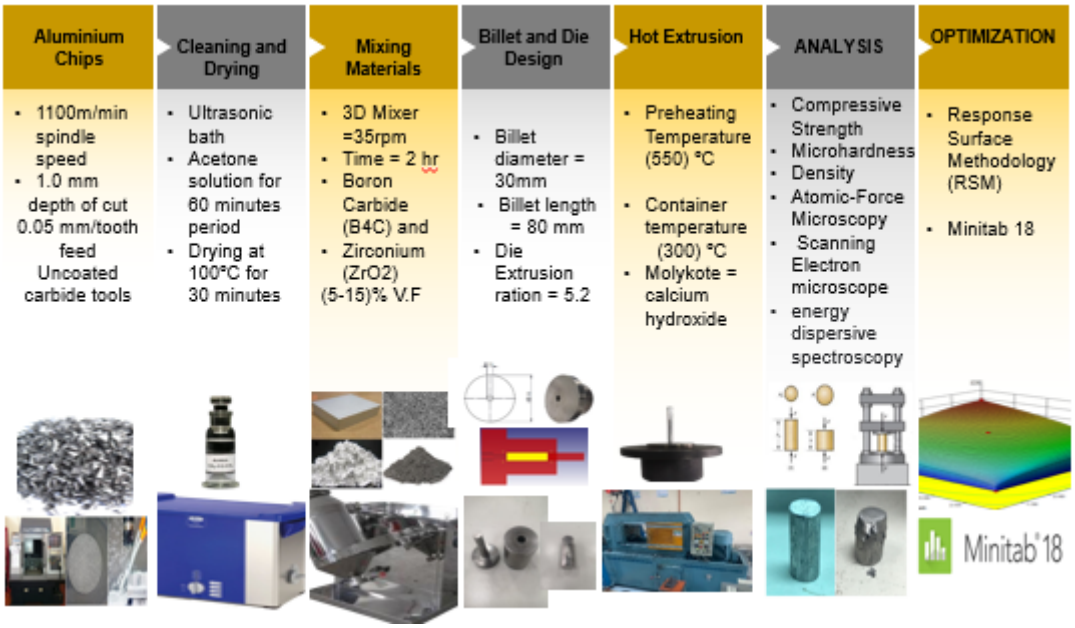

Figure 1. Experimental methods for materials preparation and characterisation.

2.3. Material Characterisation

The extruded samples were prepared following ASTM E9-09 for test of compressive strength. The density of the material was investigated and measured in the air and distilled water by employing Archimedes' principle. The investigated reinforced particles distribution, chips boundaries, and grains properties were characterised by AFM XE-100 (PSIA Corp., Sungnam, Korea) and SEM (Model No: JEOL JSM-6380la MP-19500014). Energy – dispersive X – ray spectroscopy (EDS) was conducted to investigate the distribution of the recycled composite elements.

Furthermore, microhardness investigations were conducted with a force of 0.980 N for 10 s of holding time following DIN EN ISO 6507-1:2005 standards. Five different points were measured and the uniformity of the formed materials and the mean microhardness values were recorded. The samples preparation involved sectioning, grinding, polishing, and etching. The process allowed the hybrid samples to dissolve the elevated particles above the samples and over a cleaned and dried surface to attain excellent microstructure findings. The tip of the AFM probe was very sharp, usually less than 100 Å in diameter at the end of a small cantilever. The probe was connected to a piezo scanner tube, which scanned the probe over a selected area of the sample surface. The interatomic force between the probe tip and the sample surface caused the cantilever to deflect as the sample changed the surface roughness (or other properties). The laser reflected from the back of the cantilever measured the deflection of the cantilever [28]. Table 2 shows the studied different volume fractions of the B_4C and ZrO_2 particles, which affect the recycled material structure.

Table 2. Experimental design parameters.

Factor	Variation Levels		
	Low (−1)	**Medium (0)**	**High (+1)**
Boron Carbide B_4C (%)	5	10	15
Zirconia ZrO_2 (%)	5	10	15

The design of experiment (DOE) was performed to validate the investigated parameters of 5–15% B_4C and ZrO_2 ceramic particles under a 550 °C processing temperature and

3 h preheating time. According to the Box Behnken design (BBD) method, the design introduced eight factorial points and three centre points. The purpose of applying this concept is to model and analyse the compressive strength response at a two-factor, second-order model:

$$Y = b_0 + \sum_{i=1}^{3} b_i x_i + \sum_{i=1}^{3} b_{ii} x_i^2 + \sum_{i=1}^{2} \sum_{j>i}^{3} b_{ij} x_i x_j \quad (1)$$

where b_0, b_i, b_{ii}, b_{ij}, x_i (x_j), and Y are the regression coefficients for intercept value, linear model, quadratic number, interaction, extraction factor, and outcomes response, respectively [29].

By applying a design that could fit the two-factor, second-order model, the matrix X of the reinforced material for this design is given by:

$$\begin{bmatrix} 1 & -1 & 1 & 1 & 1 & 1 \\ 1 & -1 & 1 & 1 & 1 & -1 \\ 1 & -1 & -1 & 1 & 1 & -1 \\ 1 & -1 & 1 & 1 & 1 & 1 \\ 1 & -\alpha & 0 & \alpha^2 & 0 & 0 \\ 1 & \alpha & 0 & \alpha^2 & 0 & 0 \\ 1 & 0 & -\alpha & 0 & \alpha^2 & 0 \\ 1 & 0 & \alpha & 0 & \alpha^2 & 0 \\ 1 & 0 & 0 & 0 & 0 & 0 \end{bmatrix} \quad (2)$$

$$X = \begin{bmatrix} N & 0 & 0 & a & a & 0 \\ 1 & a & 0 & 0 & 0 & 0 \\ 0 & 0 & a & 0 & 0 & 0 \\ a & 0 & 0 & b & F & 0 \\ a & 0 & 0 & F & b & 0 \\ 1 & \alpha & 0 & \alpha^2 & 0 & 0 \\ 0 & 0 & 0 & 0 & 0 & F \end{bmatrix}$$

where N is the number of experiments, F is the factorial part of the central composites design, a is the axial variable, and b is the quantity variables [29–31]. Consider

$$a = F + 2\alpha^2$$
$$b = F + 2\alpha^2 \quad (3)$$

where α is the distance from the central design and the experimental chosen value for the two-factor composites centre design. The response surface methodology (RSM) study uses a central composite design (CCD) at several points, which increases the response detection for optimum factor results. The investigated parameters are ($-\alpha$, −1, 0, +1, α) in CCD, where levels −1 and +1 show the low- and high-representation values, and $-\alpha$ and α show the low- and high-extreme values [32]. The benefits of employing factorials and central and axial designs are to determine the optimum parameters of the investigated composites materials and obtain the best compressive-strength properties [33]. The parameter settings that resulted in an optimum compressive strength were then selected for material characterisations [16,34]. The Pareto chart of the parametric standards effects is shown in Figure 2, which is obtained by the minitab 18 software. The compressive strength was mainly affected by the amount of added volume fraction of the particles and the preheating temperature. The standardised effect and the influencing factors on the compressive-strength response are the volume fraction of ZrO_2 with the processing preheating temperature. The factors that do not exceed the reference line are insignificant and can be eliminated via backward elimination to refine the model. From the minitab software analysis, Figure 3 exhibits the residual plot for compressive strength. The residual for compressive strength is almost consistent in the normal probability plot. The closeness of the graph indicates that errors are negligible since they are in the tolerable margin. The plot of re-

siduals versus fits response shows the consistency of variance in equal distribution, confirming the compressive strength's approximation once it is correlated with the DOE analysis [35].

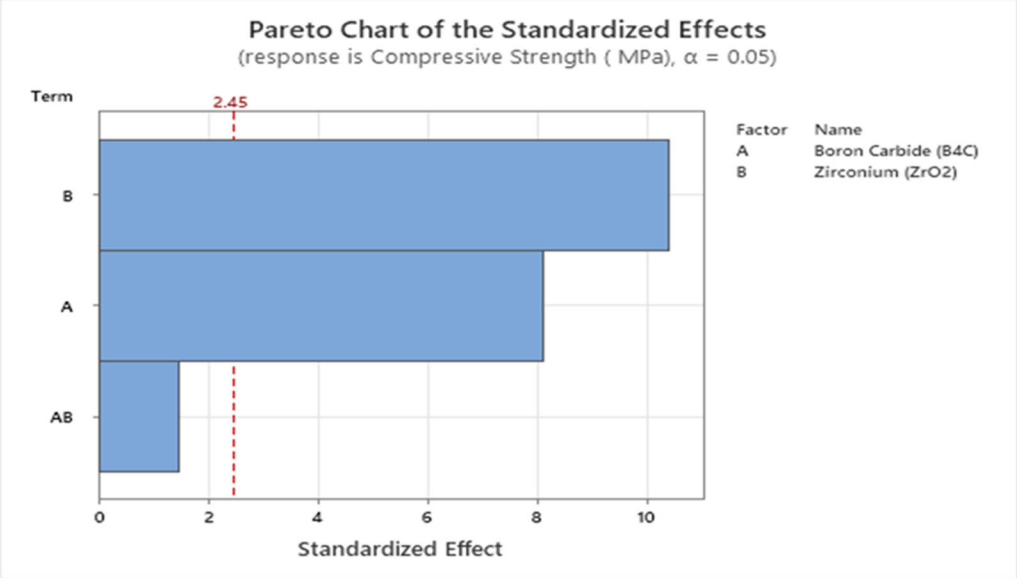

Figure 2. Pareto chart of compressive strength.

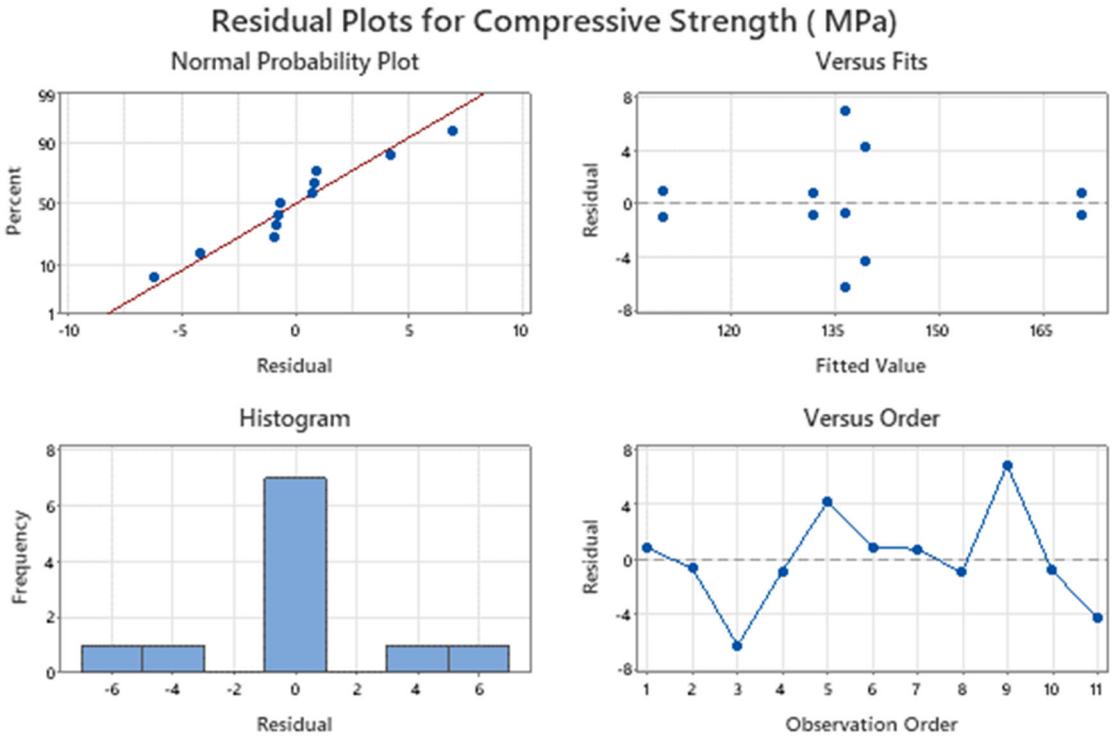

Figure 3. Residual plot of compressive strength.

The DOE analysis helps reveal relationships between process parameters and compressive-strength findings, Table 3 shows the compressive strength analysis of variance by DOE. The developed empirical model can be fully utilised to optimise the hot extrusion process. The analysis of variances (ANOVA) quadratic mathematical modelling is suggested to explain the relationship between the volume fraction of added ceramic particles and the resulting compressive strength, according to the regression model in Equation (4):

$$CS\ (\mathrm{MPa}) = 208.13 - 3.617V_{\mathrm{B_4C}} - 4.360V_{\mathrm{ZrO_2}} + 0.0966V_{\mathrm{B_4C}} \times V_{\mathrm{ZrO_2}} - 1.36\mathrm{CtPt} \quad (4)$$

where *CS* is the compressive strength, $V_{\mathrm{B_4C}}$ is the volume fraction of Boron Carbide, $V_{\mathrm{ZrO_2}}$ is the volume fraction of Zirconia, CtPt are the central points of the experiment design.

Table 3. Compressive-strength analysis of variance by DOE.

Source	DF	Adj SS	Adj MS	F-Value	*p*-Value
Model	4	3758.36	939.59	44.23	0.000
Linear	2	3707.59	1853.80	87.26	0.000
Boron Carbide (B_4C)	1	1404.77	1404.77	66.12	0.000
Zirconia (ZrO_2)	1	2302.83	2302.83	108.40	0.000
2-Way Interactions	1	46.71	46.71	2.20	0.189
Boron Carbide (B_4C) × Zirconia (ZrO_2)	1	46.71	46.71	2.20	0.189
Curvature	1	4.06	4.06	0.19	0.677
Error	6	127.47	21.24		
Total	10	3885.83			

The DOE model validated the volume fraction with a constant value of preheat temperature at 550 °C. However, the calculated *p*-value is less than the standard (p = 0.005) presented in Table 3. Hence, the model is practically correct according to the presented measurement. The values of S = 4.6092, R^2 = 96.72%, R^2 adj = 94.53%, and R^2 pred = 90.81% propose that the relationship between the processed parameters and responses have good agreement in this research, where S is an observed value and R^2 is a coefficient of determination and is adjusted (R^2 adj).

Table 4 presents the DOE design employed. It allows the experiments to be conducted at the optimum range only. Therefore, the constant range of the temperature is 550 °C, and the volume fraction of the ceramic particles was investigated under three hours of processing time. The compressive strength was increased by increasing the volume fraction up to 5%, and beyond this value, it decreased with the lowest observed compressive strength at 15% for both the B_4C and ZrO_2 volume fractions. The use of DOE investigates the range of volume fractions.

Table 4. Optimisation values over compressive-strength response.

Variable			Setting	
Boron Carbide (B_4C)			5	
Zirconia (ZrO_2)			5	
Response	**Fit**	**SE Fit**	**95% CI**	**95% PI**
Compressive Strength (MPa)	170.66	3.26	(162.69, 178.64)	(156.85, 184.48)

3. Results and Discussion

Table 5 is presented to investigate the relationship between the processed factors (B_4C and ZrO_2 particles) which affect the response outputs of the recycled aluminium. The compression tests and microhardness and density measurements were carried out. The response of compressive strength was used to predict the optimisation of different volume fractions of reinforced B_4C and ZrO_2 ceramic particles. The statical analysis was used to obtain related parameters which cause higher material strength by employing the CCD model of analysis, following the experimental design [36]. Compressive strength, micro hardness, and density are presented separately in the following sections.

Table 5. Compressive strength, microhardness, and density of hybrid materials reinforced by different volume fractions of B_4C and ZrO_2 particles.

No.	Sample Notation	B_4C (%)	ZrO_2 (%)	Density kg/m³	Hardness (VH)	Max Strain %	Compressive Strength (MPa)
1.	S1	5	5	2.65	70.65	16.477	171.44
2.	S2	15	5	2.49	65.42	13.239	143.56
3.	S3	5	15	2.62	57.55	21.669	131.07
4.	S4	15	15	2.57	55.78	11.977	111.16
5.	S5	5	5	2.65	69.83	12.130	169.89
6.	S6	15	5	2.47	55.99	11.149	135.10
7.	S7	5	15	2.62	53.02	9.531	132.73
8.	S8	15	15	2.58	55.69	10.597	109.30
9.	S9	10	10	2.6	54.43	10.497	130.41
10.	S10	10	10	2.59	61.81	15.675	136.01
11.	S11	10	10	2.59	56.27	11.555	143.58

3.1. Compressive Strength

After the DOE design experimental procedures, the samples for hot extrusion were prepared at different volume fractions of reinforced B_4C and ZrO_2 ceramic particles (5–15%) following the DOE design experimental procedures. The samples were annealed in a furnace preheated at a temperature of 550 °C for three hours for all samples. The compression strength of the interlayers recycled hybrid materials with multiple B_4C and ZrO_2 reinforced particle size ratios was compared in Figure 4. The effects of the reinforced fractions on the recycled hybrid materials were analysed. From Figure 4, the compressive strengths of the samples are gradually enhanced up to the volume fraction of 5% in each design. Beyond the 5% volume fraction, the compression strengths dropped for 10% and 15% volume fraction of the ceramic particles. Samples four and eight obtained the lowest compressive strength values at 15% of B_4C and ZrO_2 contents. This is due to the agglomeration of the particles and pores availability. Increasing the content percentage beyond 15% yields large pores and increases the voids in size, which directly affects the recycled hybrid material concentrations [37]. The highest reported values of compressive strength were samples one and five. The material properties were strengthened by producing dislocations that pile up the total work hardening of the processed deformed specimens [38]. Therefore, the compression strength differed depending on the percentage values of reinforced particles mixed to aluminium AA6061 chips during the forming process.

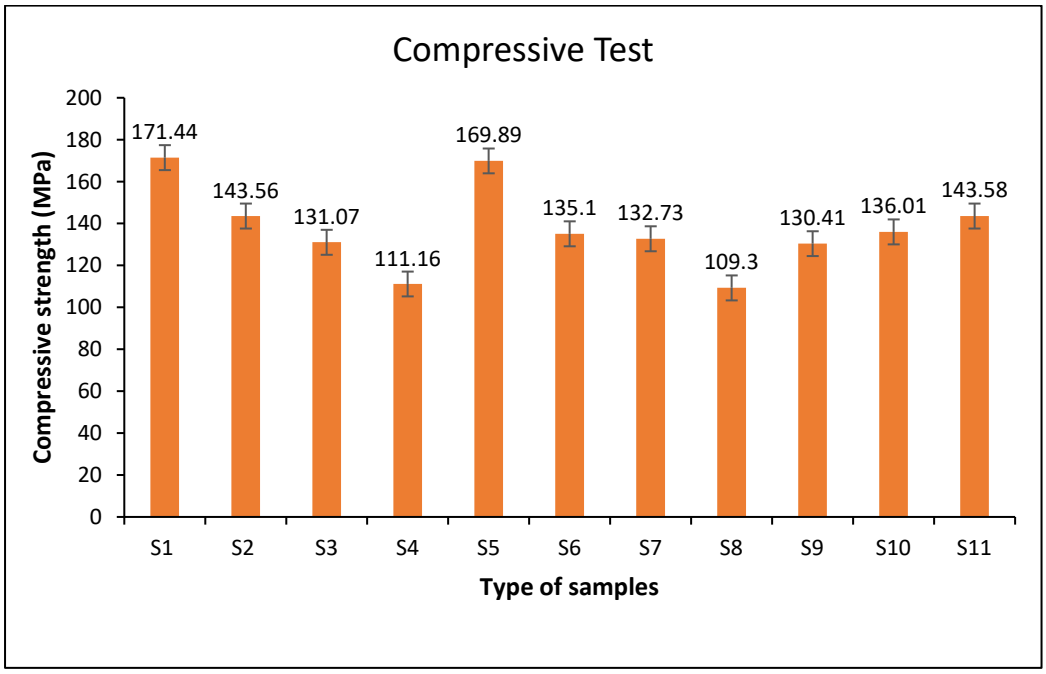

Figure 4. The compressive strength of recycled hybrid materials with reinforced B_4C and ZrO_2 particles.

3.2. Microhardness

Microhardness is the material resistance to the deformed surface localisation [39]. In general, adding ceramic contents increases the microhardness distribution values of the tested hybrid samples. From Figure 5, the microhardness increased by increasing the ceramic particles up to 5 % volume fraction (B_4C and ZrO_2). Beyond 5 % volume fraction (B_4C and ZrO_2), the microhardness declined due to the increasing pores and cracks from the material agglomeration and inhomogeneous distribution of particles [40]. It is noted that an optimum amount of ceramics particles addition of B_4C and ZrO_2 refers to their wettability, conductivity, and entrapping dislocations. According to Equation (5) [41]:

$$\lambda = 4(1 - f)r/\ 3f \quad (5)$$

where λ is the distance of reinforced particles, r is the radius of ceramic particles, and f is the volume fraction of ceramic particles. Increasing the reinforced volume fraction will decrease the distance between the added particles. Equation (6) illustrates those effects:

$$\tau_0 = (Gb\ /\ \lambda) \quad (6)$$

where τ_0 is the shearing stress, G is the shearing module, b is the Burger's crystal vector, and λ is the distance of reinforced particles. The Equations (5) and (6) conclude that the distance between particles decreases, and the shear of material dislocations would increase. This phenomenon will continue until the pores appear as a result of material agglomeration which causes low material strength. Increasing the microporosity, the discontinuity of the material phases will be greater, and the stress concentration level will be higher.

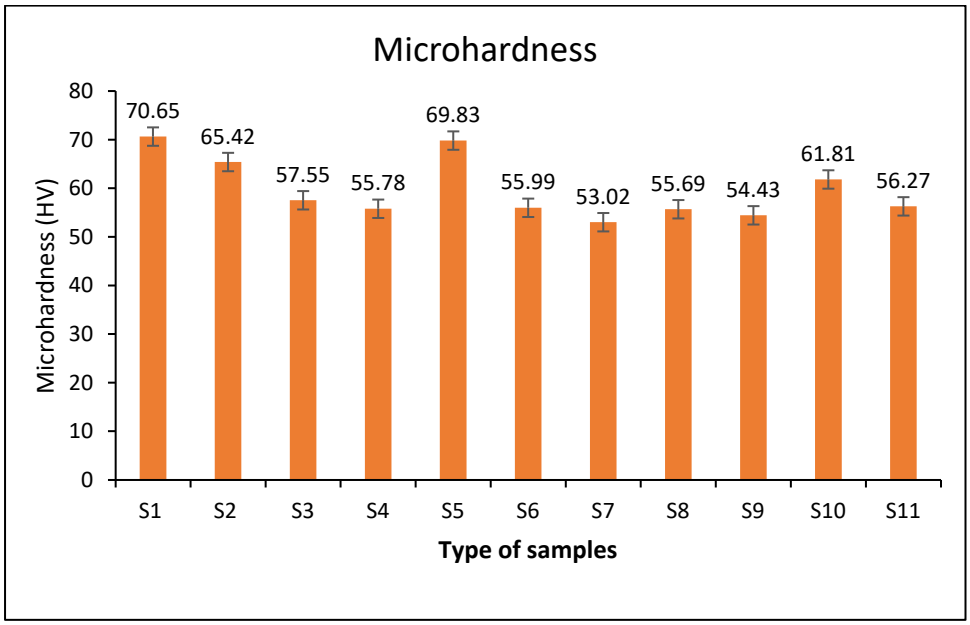

Figure 5. Microhardness of recycled hybrid materials with reinforced B_4C and ZrO_2 particles.

3.3. Density

The samples for density tests were 10 mm × 10 mm × 10 mm, calculated using Archimedes' principle under different conditions in the air and water. The density values were increased as a result of increasing the preheating processing temperature. This is because ZrO_2 particles have a high density of 5.68 g/cm^3 which increases the total density of the recycled hybrid materials, while increasing the B_4C particles results in a decrease in the density of recycled materials because B_4C particles have a lower density of 2.52 g/cm^3. As shown in Figure 6, the density reduction was compensated as a result of the extrusion-processing temperature. This is because activation energy requires the temperature derivation of the lead mechanism to the neck growth under the effects of thermal-processing surface and volume diffusion [36]. The recycled hybrid materials were characterised by localised plastic deformation in the matrix at a 550 °C processing temperature. The processing temperature causes cracking at grain boundaries which coalesce during repeated loading fracture. Therefore, the accumulation of thermal gradient stresses of the recycled hybrid materials yields density dislocation at a high-processing temperature [42,43].

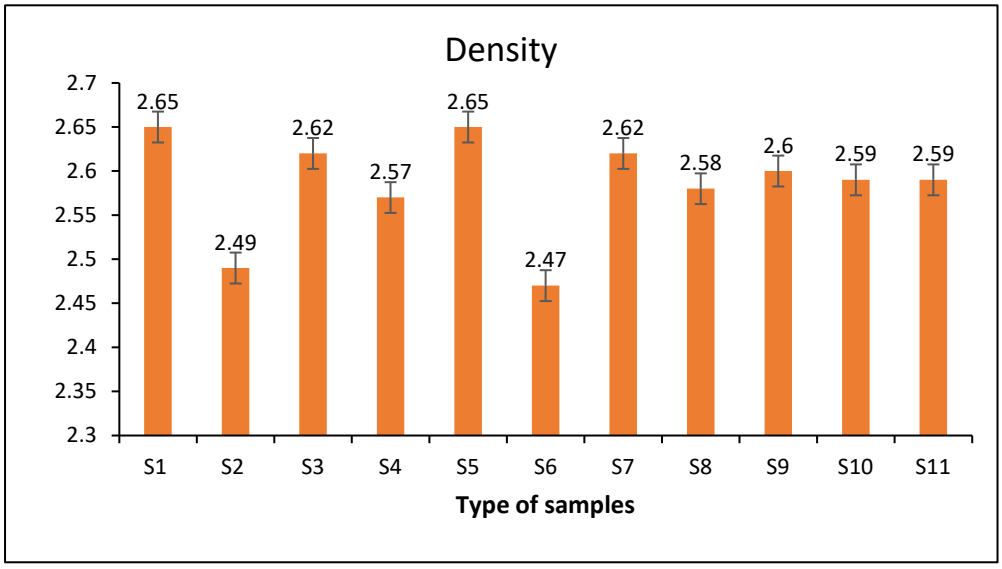

Figure 6. The density of recycled hybrid materials B_4C and ZrO_2 reinforced.

3.4. Metallographic FE-SEM and AFM Analysis

The metallographic analysis is a good investigation tool for microstructural research of recycled metals in composites or hybrid forms. The selected samples of different mix percentages of ZrO_2 and B_4C reinforced ceramic particles with AA6061 chips have been investigated. Figure 7 shows that development of most grains occurred within the deformation die due to die shear stress, strain, and applied preheating temperature. The processed chips with reinforced particles have been elongated and transformed into fine weld lines. This is due to the broken oxide layers that form fine fragments of oxide layers [15]. Figure 7 presents that the fine fragments oxide layers are homogenously distributed within the extruded workpiece structures and have a good weld line that results in good compressive strength. In addition, the effects of adding ZrO_2 and B_4C ceramic particles cause the growth of the grains' boundary region. However, a higher concentration of reinforced ceramic particles beyond the optimised parameters could cause more agglomeration of particles and greater grains. Hence, a higher level of processing temperature of 550 °C is participating to bond the surrounding aluminium chips in less solidification time. Increasing the solidification time leads to poor distribution of ceramic particles in the stage of bonding chips and particles at the solidified zone [41].

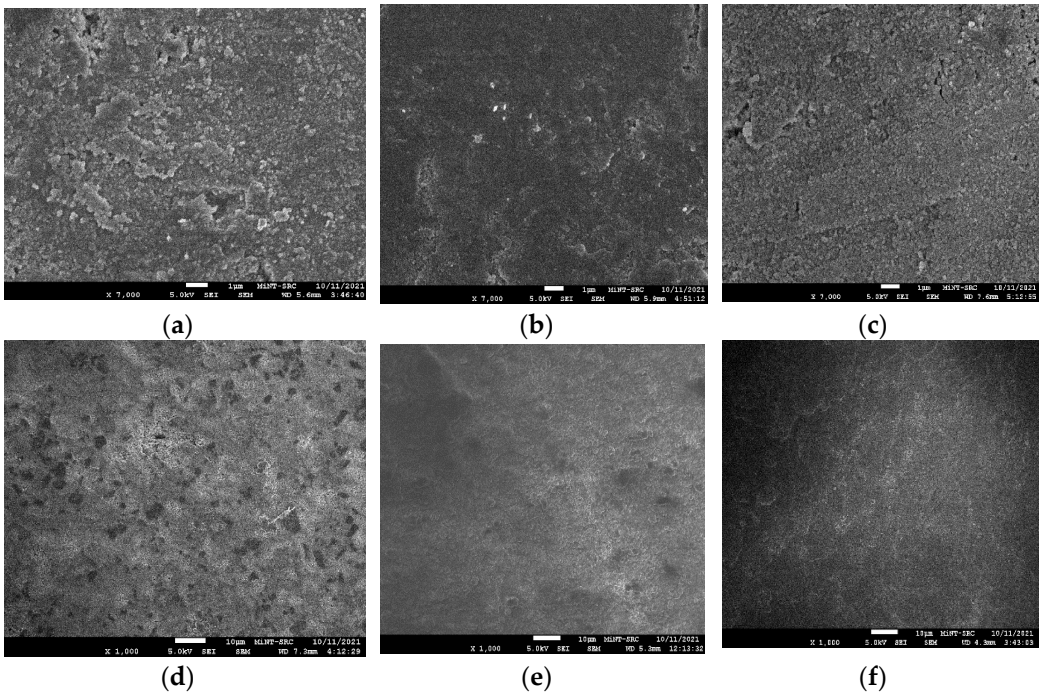

Figure 7. FE-SEM images of the investigated: (**a**) Al/5% B_4C-5% ZrO_2, (**b**) Al/15% B_4C-15% ZrO_2, (**c**) Al/10% B_4C-10% ZrO_2, (**d**) Al/5% B_4C-15% ZrO_2, (**e**) Al/15% B_4C/5% ZrO_2 samples, and (**f**) Al-chips.

AFM scanning was introduced to investigate the problems of cantilevers along the material surface. The material-profiling deflection was measured with 3D profile at a magnification of a million times. It is necessary to show the material topography compared to optical scanning microscopes. This presentation shows the material combination of B_4C, ZrO_2 particles with AA6061 hybrid materials in terms of roughness and 3D surfaces profiles [28,44]. AFM was introduced to show the agglomeration of recycled hybrid materials under 550 °C preheating temperature. The results were altered during the hot-extrusion process depending on the added B_4C and ZrO_2 ceramics particles. Table 6 summarises effects of AFM mean area, volume, and length on surface roughness; it shows that the grains were less distributed depending on the extra volume fraction of the added particles. Hence, measuring grains exhibited the thin film's polycrystalline structure dependents of ceramic particles to the aluminium chips, as presented in Figure 8. The thin films

kept decreasing all the grain's length as the root mean square because of the enlargement added particles time growth. Thus, the decrease in the film's thickness causes a decrease in the surface of the hybrid material characterisations [45].

Table 6. Effects of AFM mean area, volume, and length on surface roughness.

Samples	Grain Area (μm²)	Grain Volume (μm²)	Grain Length (μm²)	Rq	Ra
Al/5% B_4C-5% ZrO_2	0.026	0.001	0.228	11.85	9.36
Al/15 B_4C-15 %ZrO_2	0.041	0.002	0.232	8.70	6.77
Al/10 %B_4C-10 %ZrO_2	0.024	0.001	0.221	14.06	11.03
Al/5 %B_4C/15 %ZrO_2	0.033	0.001	0.257	10.70	8.37
Al/15 %B_4C/5 %ZrO_2	0.025	0.001	0.226	15.27	12.11
Al-chips	0.038	0.002	0.282	14.24	11.24

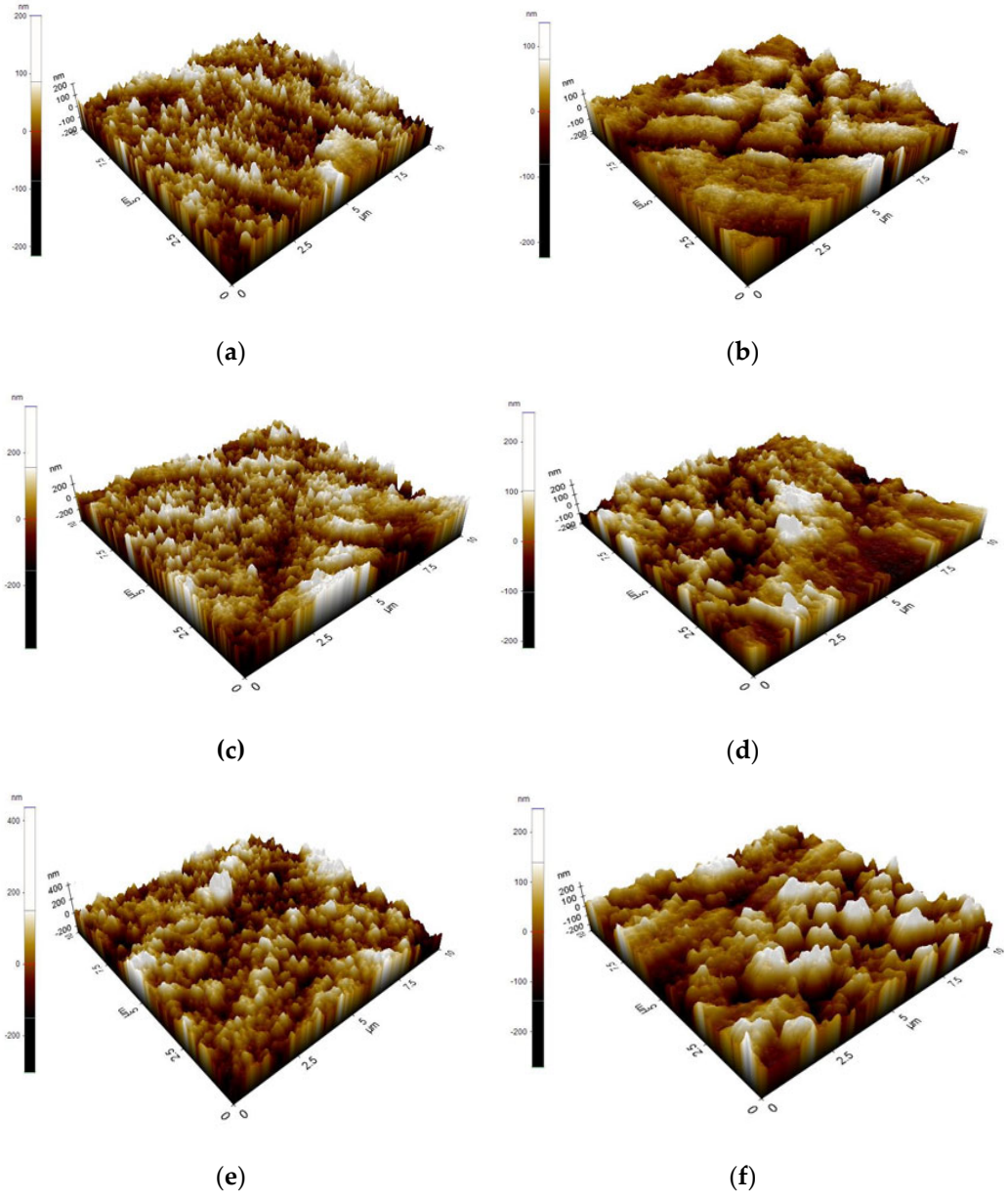

Figure 8. AFM images of the investigated: (**a**) Al/5% B_4C − 5% ZrO_2, (**b**) Al/15% B_4C − 15% ZrO_2, (**c**) Al/10% B_4C − 10% ZrO_2, (**d**) Al/5% B_4C − 15% ZrO_2, (**e**) Al/15% B_4C/5% ZrO_2 samples, and (**f**) Al − chips.

To estimate the distribution of chemical elements, energy-dispersive X-ray spectroscopy (EDS) was conducted, which has been a widely applied technique [46]. The X-ray spectroscopy results showing the distribution of material chemical elements are presented in Figure 9 and Table 7. The agglomeration of reinforced particles, such as C, O, Si, and Mg, was not removed by processing treatments and was contaminated with the Al matrix. The Al matrix and other elements incorporated during the forming process cause smaller grains depending on the kinetic reactions of the elements' composites. Poovazhagan et al. [47] and Fang et al. [48] showed that the presence of reinforced particles elements had direct effects on the microstructures of the material solidification, and they confirmed the possible chemical reactions between the process and workpiece substances of the contents.

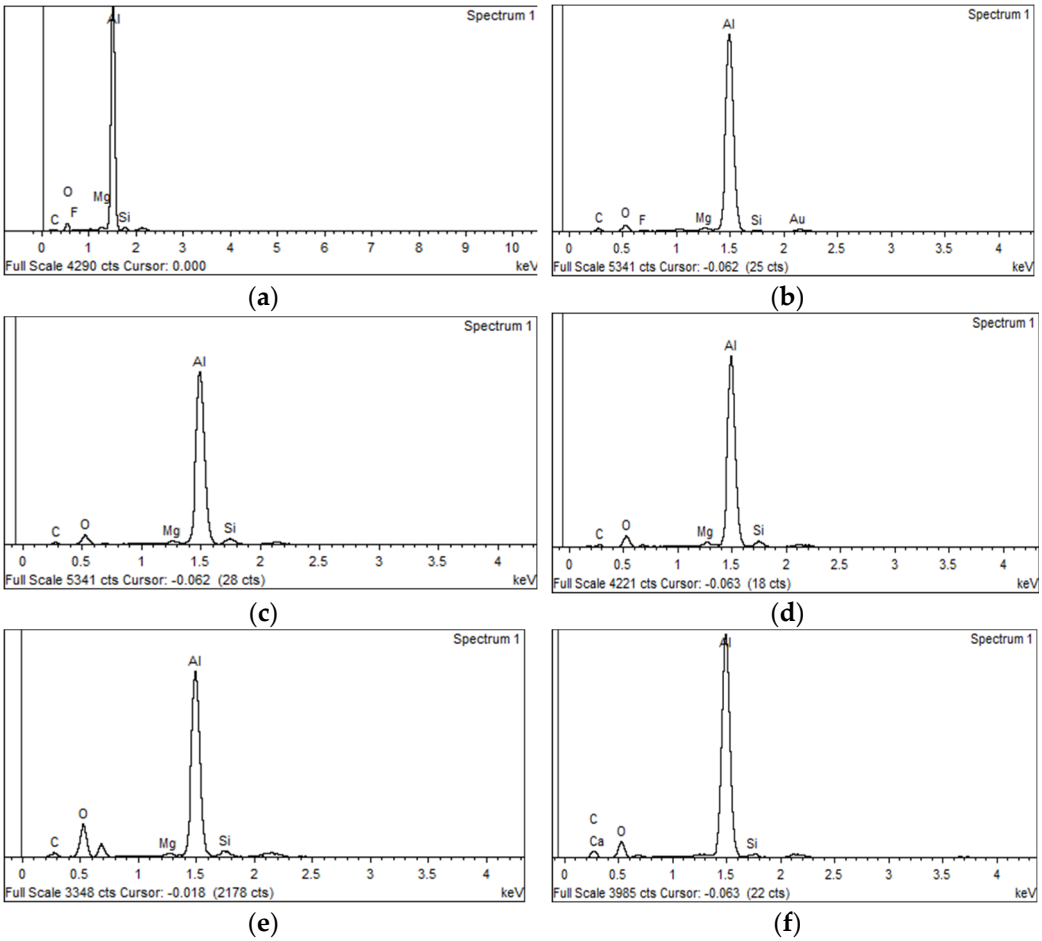

Figure 9. EDS images of the investigated: (**a**) Al/5% B_4C − 5% ZrO_2, (**b**) Al/15% B_4C − 15% ZrO_2, (**c**) Al/10% B_4C − 10% ZrO_2, (**d**) Al/5% B_4C − 15% ZrO_2, (**e**) Al/15% B_4C/5% ZrO_2 samples, and (**f**) Al − chips.

Table 7. Detailed EDS elements analysis of the investigated samples.

Samples Type	Elements					
Al/5% B_4C − 5% ZrO_2	Element	C	O	Mg	Al	Si
	Weight %	7.29	12.42	0.69	75.58	2.47
	Atomic %	13.85	17.72	0.65	63.92	2.00
Al/15% B_4C − 15% ZrO_2	Element	C	O	Mg	Al	Si
	Weight %	19.75	10.47	0.72	62.36	0.60
	Atomic %	34.53	13.74	0.62	48.54	0.45
Al/10% B_4C − 10% ZrO_2	Element	C	O	Mg	Al	Si
	Weight %	14.94	16.23	0.95	63.76	4.12

	Atomic %	25.88	21.10	0.81	49.16	3.05
	Element	C	O	Mg	Al	Si
Al/5% B_4C/15% ZrO_2	Weight %	16.14	14.73	0.67	66.41	2.05
	Atomic %	27.85	19.07	0.57	51.00	1.51
	Element	C	O	Mg	Al	Si
Al/15% B_4C/5% ZrO_2	Weight %	15.80	33.19	0.54	48.16	2.31
	Atomic %	24.91	39.29	0.42	33.81	1.56
	Element	C	O	Mg	Al	Si
Al – chips	Weight %	23.33	19.70	-	54.99	1.44
	Atomic %	36.81	23.34	-	54.99	1.44

4. Conclusions

This paper presents the investigations conducted on aluminium AA6061 chips reinforced with B_4C- and ZrO_2-based ceramic particles, which became AA6061-B_4C/ZrO_2 composites. The composite was assessed for its durability and restorative, mechanical, and physical properties. The B_4C and ZrO_2 parameters were validated by employing DOE under a 550 °C preheating temperature. The solid-state recycling of hybrid materials by hot extrusion was also conducted using the central composite design. The ANOVA revealed that factor A (B_4C) and factor B (ZrO_2) volume fractions were the most influential parameters for all responses. The combination of AB (volume fractions) directly affects the empirical model's accuracy between the predicted and actual values. The physical and microstructure have good agreement with compressive strength and hardness. Thus, increasing the volume fractions up to 5% of each reinforced ceramic particle enhanced the hybrid material properties. Higher percentages only caused inhomogeneity and decreased the properties due to particles distribution and agglomeration. Additional investigations, such as heat treatment and fatigue tests, are highly recommended for the determination of the hybrid material's mechanical and microstructure properties.

Author Contributions: Conceptualization, W.Z. and S.A.-A.; methodology, W.Z. and S.A.-A.; software, S.A.-A.; validation, S.A.-A.; formal analysis, S.A.-A.; investigation, S.A.-A., W.Z., S.S. (Shazarel Shamsudin), M.A.L., D.H.D., and Z.H.; resources, W.Z. and N.K.Y.; data curation, S.S. (Safwan Sadeq), Y.S., A.W., and S.S. (Shazarel Shamsudin); writing—original draft preparation, S.A.-A.; writing—review and editing, W.Z., D.H.D., and Z.H.; visualization, S.A.-A. and W.Z.; supervision, M.A.L. and W.Z.; project administration, S.S. (Shazarel Shamsudin). All authors have read and agreed to the published version of the manuscript.

Funding: This research received no external funding.

Institutional Review Board Statement: Not applicable.

Informed Consent Statement: Not applicable.

Data Availability Statement: The data presented in this study are available on request from the corresponding author.

Acknowledgments: The authors would like to express their deepest appreciation to the supplementary provisions provided by Sustainable Manufacturing and Recycling Technology, Advanced Manufacturing and Materials Center (SMART-AMMC), and Research Management Centre Universiti Tun Hussein Onn Malaysia (UTHM). This research was funded by the Ministry of Education (MOE) through the Fundamental Research Grant (Prototype For Direct Recycling Aircraft Grade Aluminium Using Rapid Hot Press Forging (rhpf)).

Conflicts of Interest: The authors declare no conflicts of interest.

References

1. Abbas, A.T.; Taha, M.A.; Ragab, A.E.; El-Danaf, E.A.; Abd El Aal, M.I. Effect of Equal Channel Angular Pressing on the Surface Roughness of Solid State Recycled Aluminum Alloy 6061 Chips. *Adv. Mater. Sci. Eng.* **2017**, *2017*, 5131403. https://doi.org/10.1155/2017/5131403.
2. Tekkaya, A.E.; Schikorra, M.; Becker, D.; Biermann, D.; Hammer, N.; Pantke, K. Hot profile extrusion of AA-6060 aluminum chips. *J. Mater. Process. Technol.* **2009**, *209*, 3343–3350. https://doi.org/10.1016/j.jmatprotec.2008.07.047.
3. Haase, M.; Tekkaya, A.E. Recycling of aluminum chips by hot extrusion with subsequent cold extrusion. *Procedia Eng.* **2014**, *81*, 652–657. https://doi.org/10.1016/j.proeng.2014.10.055.
4. Zhou, W.; Shao, Z.; Yu, J.; Lin, J. Advances and trends in forming curved extrusion profiles. *Materials* **2021**, *14*, 1603. https://doi.org/10.3390/ma14071603.
5. Zhou, W.; Shi, Z.; Lin, J.; Dean, T.A. Dean. An upper bound solution for deformation field analysis in differential velocity sideways extrusion using a unified stream function. *Int. J. Mech. Sci.* **2022**, *224*, 107323. https://doi.org/10.1016/j.ijmecsci.2022.107323.
6. Chmura, W.; Gronostajski, Z. Bearing composites made from aluminium and aluminium bronze chips. *J. Mater. Process. Technol.* **2006**, *178*, 188–193. https://doi.org/10.1016/j.jmatprotec.2006.03.156.
7. Rebhi, A.; Makhlouf, T.; Njah, N. X-ray diffraction analysis of 99.1% recycled aluminium subjected to equal channel angular extrusion. *Phys. Procedia* **2009**, *2*, 1263–1270. https://doi.org/10.1016/j.phpro.2009.11.090.
8. Zhou, W.; Yu, J.; Lin, J.; Dean, T.A. Effects of die land length and geometry on curvature and effective strain of profiles produced by a novel sideways extrusion process. *J. Mater. Process. Technol.* **2020**, *282*, 116682. https://doi.org/10.1016/j.jmatprotec.2020.116682.
9. Shamsudin, S.; Lajis, M.; Zhong, Z.W. Evolutionary in Solid State Recycling Techniques of Aluminium: A review. *Procedia CIRP* **2016**, *40*, 256–261. https://doi.org/10.1016/j.procir.2016.01.117.
10. Sabbar, H.M.; Leman, Z.; Shamsudin, S.B.; Tahir, S.M.; Aiza Jaafar, C.N.; Hanim, M.A.A.; Ismsrrubie, Z.N.; Al-Alimi, S. AA7075-ZrO_2 Nanocomposites Produced by the Consecutive Solid-State Process: A Review of Characterisation and Potential Applications. *Metals* **2021**, *11*, 805. https://doi.org/10.3390/met11050805.
11. Zhou, W.; Lin, J.; Dean, T.A.; Wang, L. Feasibility studies of a novel extrusion process for curved profiles: Experimentation and modelling. *Int. J. Mach. Tools Manuf.* **2018**, *126*, 27–43. https://doi.org/10.1016/j.ijmachtools.2017.12.001.
12. Zhou, W.; Yu, J.; Lin, J.; Dean, T.A. Manufacturing a curved profile with fine grains and high strength by differential velocity sideways extrusion. *Int. J. Mach. Tools Manuf.* **2019**, *140*, 77–88. https://doi.org/10.1016/j.ijmachtools.2019.03.002.
13. Zhou, W.; Yu, J.; Lu, X.; Lin, J.; Dean, T.A. A comparative study on deformation mechanisms, microstructures and mechanical properties of wide thin-ribbed sections formed by sideways and forward extrusion. *Int. J. Mach. Tools Manuf.* **2021**, *168*, 103771, 2021. https://doi.org/10.1016/j.ijmachtools.2021.103771.
14. Zhou, W.; Lin, J.; Balint, D.S.; Dean, T.A. Clarification of the effect of temperature and strain rate on workpiece deformation behaviour in metal forming processes. *Int. J. Mach. Tools Manuf.* **2021**, *171*, 103815, 2021. https://doi.org/10.1016/j.ijmachtools.2021.103815.
15. Güley, V.; Güzel, A.; Jäger, A.; Ben Khalifa, N.; Tekkaya, A.E.; Misiolek, W.Z. Effect of die design on the welding quality during solid state recycling of AA6060 chips by hot extrusion. *Mater. Sci. Eng. A* **2013**, *574*, 163–175. https://doi.org/10.1016/j.msea.2013.03.010.
16. Blindheim, J.; Grong, Ø.; Aakenes, U.R.; Welo, T.; Steinert, M. Hybrid Metal Extrusion & Bonding (HYB)—A new technology for solid-state additive manufacturing of aluminium components. *Procedia Manuf.* **2018**, *26*, 782–789. https://doi.org/10.1016/j.promfg.2018.07.092.
17. Sanusi, K.O.; Makinde, O.D.; Oliver, G.J. Equal channel angular pressing technique for the formation of ultra-fine grained structures. *South Afr. J. Sci.* **2012**, *108*, 1–7. https://doi.org/10.4102/sajs.v108i9/10.212.
18. Rezaei, M.R.; Shabestari, S.G.; Razavi, S.H. Effect of ECAP consolidation temperature on the microstructure and mechanical properties of Al-Cu-Ti metallic glass reinforced aluminum matrix composite. *J. Mater. Sci. Technol.* **2017**, *33*, 1031–1038. https://doi.org/10.1016/j.jmst.2016.10.013.
19. Zhou, P.; Wang, H.; Nie, H.; Cheng, W.; Niu, X.; Wang, Z.; Liang, W. Effect of ECAP temperature on precipitation and strengthening mechanisms of Mg–9Al–1Si alloys. *J. Mater. Res.* **2018**, *33*, 1822–1829. https://doi.org/10.1557/jmr.2018.137.
20. Nie, C.; Gu, J.; Liu, J.; Zhang, D. Production of Boron Carbide Reinforced 2024 Aluminum Matrix Composites by Mechanical Alloying. *Mater. Trans.* **2007**, *48*, 990–995. https://doi.org/10.2320/matertrans.48.990.
21. Fogagnolo, J.B.; Ruiz-Navas, E.M.; Simón, M.A.; Martinez, M.A. Recycling of aluminium alloy and aluminium matrix composite chips by pressing and hot extrusion. *J. Mater. Process. Technol.* **2003**, *143–144*, 792–795. https://doi.org/10.1016/S0924-0136(03)00380-7.
22. Qi, Y.; Kosinova, A.; Lakin, E.; Popov, V.V., Jr.; Rabkin, E.; Lapovok, R. Effect of SPD Processing on the Strength and Conductivity of AA6061 Alloy. *Adv. Eng. Mater.* **2019**, *21*, 1801370. https://doi.org/10.1002/adem.201801370.
23. Larianovsky, N.; Popov, V.; Katz-Demyanetz, A.; Fleisher, A.; Meyers, D.E.; Chaudhuri, R.S. Production of Al Metal Matrix Composites Reinforced with Carbon Nanotubes by Two-Stage Melt-Based HPDC-CE Method. *J. Eng. Mater. Technol.* **2019**, *141*, 011002. https://doi.org/10.1115/1.4040556.
24. Murthy, I.N.; Babu, N.A.; Rao, J.B. Comparative Studies on Microstructure and Mechanical Properties of Granulated Blast Furnace Slag and Fly Ash Reinforced AA 2024 Composites. *J. Miner. Mater. Charact. Eng.* **2014**, *2*, 319–333.

25. Al-Alimi, S.; Lajis, M.A.; Shamsudin, S.; Chan, B.L.; Mohammed, Y.; Ismail, A.E.; Sultan, N.M. Development of metal matrix composites and related forming techniques by direct recycling of light metals: A review. *Int. J. Integr. Eng.* **2020**, *12*, 144–171.
26. Derakhshandeh-Haghighi, R.; Jenabali Jahromi, S.A. The Effect of Multi-pass Equal-Channel Angular Pressing (ECAP) for Consolidation of Aluminum-Nano Alumina Composite Powder on Wear Resistance. *J. Mater. Eng. Perform.* **2016**, *25*, 687–696. https://doi.org/10.1007/s11665-016-1888-8.
27. Yerbolat, G.; Amangeldi, S.; Ali, M.H.; Badanova, N.; Ashirbeok, A.; Islam, G. Composite materials property determination by Rule of Mixture and Monte Carlo Simulation. In Proceedings of the 2018 IEEE International Conference on Advanced Manufacturing (ICAM), Yunlin, Taiwan, 16–18 November 2018; pp. 384–387. https://doi.org/10.1109/AMCON.2018.8615034.
28. Aliofkhazraei, M.; Ali, N. *AFM Applications in Micro/Nanostructured Coatings*; Elsevier: Amsterdam, The Netherlands, 2014; Volume 7; ISBN 9780080965338.
29. Khuri, A.I.; Mukhopadhyay, S. Response surface methodology. *Wiley Interdiscip. Rev. Comput. Stat.* **2010**, *2*, 128–149. https://doi.org/10.1002/wics.73.
30. Peasura, P. Application of Response Surface Methodology for Modeling of Postweld Heat Treatment Process in a Pressure Vessel Steel ASTM A516 Grade 70. *Sci. World J.* **2015**, *2015*, 318475.
31. Zhou, W.; Xi, Z. Bending Behaviour Analysis of Aluminium Profiles in Differential Velocity Sideways Extrusion Using a General Flow Field Model. *Metals* **2022**, *12*, 877. https://doi.org/10.3390/met12050877.
32. Nemati-chari, R.; Dehghani, K.; Kami, A.; Banabic, D. Application of Response Surface Methodology for Study of Effective Strain in Equal Channel Angular Pressing of Aa6061 Alloy. *Proc. Rom. Acad. Ser. A* **2015**, *16*, 217–225.
33. Penjumras, P.; Abdul Rahman, R.; Talib, R.A.; Abdan, K. Response Surface Methodology for the Optimization of Preparation of Biocomposites Based on Poly(lactic acid) and Durian Peel Cellulose. *Sci. World J.* **2015**, *2015*, 293609. https://doi.org/10.1155/2015/293609.
34. Al-Alimi, S.A.M.; Bin Lajis, M.A.; Bin Shamsudin, S.; Long, C.B. Influence of Zirconia Percent on Physical Properties of Zirconia—Aluminum Chip Matrix (Al6061) Nanocomposites. *J. Nanostructures* **2022**, *12*, 194–203. https://doi.org/10.22052/JNS.2022.01.018.
35. Sarabia, L.A.; Ortiz, M.C. Response Surface Methodology. 1.12—Response Surface Methodology. In *Comprehensive Chemometrics*; Elsevier: Oxford, UK, 2009; pp. 345–390. https://doi.org/10.1016/B978-044452701-1.00083-1.
36. Msebawi, M.S.; Leman, Z.; Shamsudin, S.; Tahir, S.M.; Aiza Jaafar, C.N.; Ariff, A.H.M.; Zahari, N.I.; Abdellatif, A. Production of Aluminum AA6061 Hybrid Nanocomposite from Waste Metal Using Hot Extrusion Process: Strength Performance and Prediction by RSM and Random Forest. *Materials* **2021**, *14*, 6102. https://doi.org/10.3390/ma14206102.
37. Ramnath, B.V.; Elanchezhian, C.; Annamalai, R.M.; Aravind, S.; Atreya, T.S.A.; Vignesh, V.; Subramanian, C. Aluminium metal matrix composites—A review. *Rev. Adv. Mater. Sci.* **2014**, *38*, 55–60.
38. Al-Alimi, S.; Lajis, M.A.; Shamsudin, S.; Yusuf, N.K.; Chan, B.L.; Didane, D.H.; Rady, M.H.; Sabbar, H.M.; Msebawi, M.S. Development of Hot Equal Channel Angular Processing (ECAP) Consolidation Technique in the Production of Boron Carbide(B4C)-Reinforced Aluminium Chip (AA6061)-Based Composite. *Int. J. Renew. Energy Dev.* **2021**, *10*, 607–621. https://doi.org/10.14710/ijred.2021.33942.
39. Rino, J.J.; Chandramohan, D.; Sucitharan, K.S. An Overview on Development of Aluminium Metal Matrix Composites with Hybrid Reinforcement. *Int. J. Sci. Res.* **2012**, *1*, 196–203.
40. Xu, C.; Langdon, T.G. The development of hardness homogeneity in aluminum and an aluminum alloy processed by ECAP. *J. Mater. Sci.* **2007**, *42*, 1542–1550. https://doi.org/10.1007/s10853-006-0899-5.
41. Shirvanimoghaddam, K.; Khayyam, H.; Abdizadeh, H.; Karbalaei Akbari, M.; Pakseresht, A.H.; Abdi, F.; Abbasi, A.; Naebe, M. Effect of B4C, TiB_2 and $ZrSiO_4$ ceramic particles on mechanical properties of aluminium matrix composites: Experimental investigation and predictive modelling. *Ceram. Int.* **2016**, *42*, 6206–6220. https://doi.org/10.1016/j.ceramint.2015.12.181.
42. Oladijo, O.P.; Awe, S.A.; Akinlabi, E.T.; Phiri, R.R.; Collieus, L.L.; Phuti, R.E. High-Temperature Properties of Metal Matrix Composites. *Encycl. Mater. Compos.* **2021**, 360–374. https://doi.org/10.1016/b978-0-12-819724-0.00096-3.
43. Oñoro, J.; Salvador, M.D.; Cambronero, L.E.G. High-temperature mechanical properties of aluminium alloys reinforced with boron carbide particles. *Mater. Sci. Eng. A* **2009**, *499*, 421–426. https://doi.org/10.1016/j.msea.2008.09.013.
44. Bony, A. AFM characterization of the shape of surface structures with localization factor. *Micron* **2016**, *87*, 1–9.
45. Borblik, V.; Korchevoi, A.; Nikolenko, A.; Strelchuk, V.; Fonkich, A. Fabrication of Nanostructured Objects by Thermal Vacuum Deposition of Ge Fabrication of Nanostructured Objects by Thermal Vacuum Deposition of Ge Films onto (100) GaAs Substrates. *Nanosci. Nanoeng.* **2016**, *4*, 22–30. https://doi.org/10.13189/nn.2016.040103.
46. Faizov, S.; Sarafanov, A.; Erdakov, I.; Gromov, D.; Svistun, A.; Glebov, L.; Bykov, V.; Bryk, A.; Radionova, L. On the direct extrusion of solder wire from 52in-48sn alloy. *Machines* **2021**, *9*, 93. https://doi.org/10.3390/machines9050093.
47. Poovazhagan, L.; Kalaichelvan, K.; Rajadurai, A.; Senthilvelan, V. Characterization of hybrid silicon carbide and boron carbide nanoparticles-reinforced aluminum alloy composites. *Procedia Eng.* **2013**, *64*, 681–689. https://doi.org/10.1016/j.proeng.2013.09.143.
48. Fang, D.R.; Zhang, Z.F.; Wu, S.D.; Huang, C.X.; Zhang, H.; Zhao, N.Q.; Li, J.J. Effect of equal channel angular pressing on tensile properties and fracture modes of casting Al–Cu alloys. *Mater. Sci. Eng. A* **2006**, *426*, 305–313. https://doi.org/10.1016/j.msea.2006.04.044.